Improved Large-Signal Model and Model Extraction Procedure for InGaP/GaAs HBTs under High-Current Operations

Sergey V. Cherepko, Mikhail S. Shirokov and James C. M. Hwang
Lehigh University, Bethlehem, PA 18015 USA
Alan Brandstaedter
Anadigics, Inc., Warren, NJ 07059 USA

***Abstract* — Improved large-signal as well as improved model extraction procedure is proposed for InGaP/GaAs HBTs under high-current operations. The model comprises physics-based differential equations that are implemented through symbolically defined devices in a commercially available circuit simulator. Other model improvements include bi-lateral logical correlation with small-signal characteristics, and additional series resistance with the base-emitter diffusion capacitance. The improvement in extraction procedure is mainly based on a fixed intrinsic vs. extrinsic base-collector capacitance ratio at low currents, whereas a fixed intrinsic base resistance at high currents. Experimentally it has been verified that the as-extracted model without numerical optimization closely predicts the RF power performance of the HBTs.**

I. INTRODUCTION

Unlike the case of GaAs FETs or Si BJTs, large-signal modeling of GaAs HBTs has yet to mature to the degree that a standard model is widely accepted and the model extraction procedure is automatic. Recently, we attempted to thoroughly characterize the high-current effects of InGaP/GaAs HBTs, but arrived at a large-signal model that contained non-physical trans-capacitances and was too cumbersome to be extracted directly [1]. This paper reports the improvements over [1] in both the model and the extraction procedure.

The model and extraction procedure were validated on InGaP/GaAs HBTs that were fabricated by another foundry. Each HBT has a single emitter 3 μm wide and 20 μm long. After the HBT wafers were fabricated, they were thinned to approximately 100 μm. Via grounding was made though the substrate. Chips containing discrete HBTs were diced and mounted on metal carriers. Dc and RF tests were made by using microwave wafer probes. The forward current gain cutoff frequency is typically 40 GHz. The maximum frequency of oscillation is typically 30 GHz in a 50 Ω system.

II. DC MODEL

Fig. 1 shows the dc equivalent circuit model. It uses standard Π-topology with different diode-like current sources representing different junction current components. Voltage dependence of these current sources follows that of ideal *pn*-junctions with temperature-dependent ideality factors:

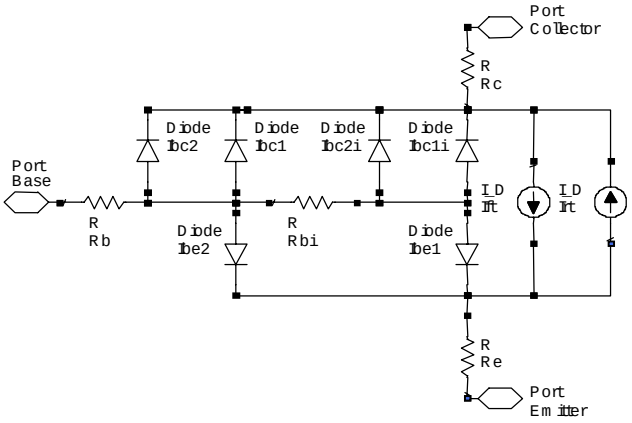

Fig. 1 DC equivalent circuit model.

$$I = I_0 \cdot e^{-\frac{V_A}{V_T}} \cdot \left(e^{\frac{V}{(n_0 + \delta_N T_J) V_T}} - 1 \right) \qquad (1)$$

where I_0 is the pre-exponential factor, qV_A is the activation energy of the saturation current, V_T is the thermal voltage, n_0 is the ideality factor at 0 K, δ_N defines the temperature dependence of the ideality factor, and T_J is the junction temperature in K.

Forward and reverse transport currents I_{FT} and I_{RT} have close-to-unity ideality factors. They share the same set of I_0, V_A, n_0 and δ_N with the ideal components of base-emitter and base-collector currents (I_{BE1} and I_{BC1}). Non-ideal component I_{BE2} and I_{BC2} each uses a separate set of parameters (see Table I). Both ideal and non-ideal base-collector currents are further separated into intrinsic and extrinsic components according to a geometric factor X_{BC}.

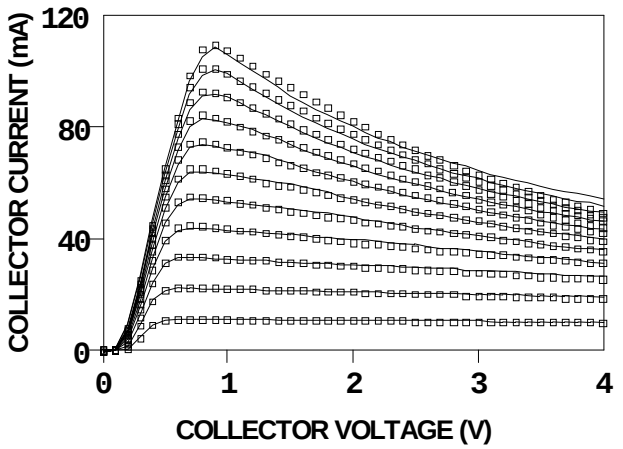

Fig. 2 (—) Simulated vs. (□) measured collector characteristics. I_B = 75, 150 ... 875 μA. Case temperature = 10°C.

$$
\begin{aligned}
&I_{FT} = I_T(V_{BEi}), \quad I_{RT} = I_T(V_{BCi}) \\
&I_{BC1i} = (1 - X_{BC}) \cdot I_{RT} / \beta_R \\
&I_{BC2i} = (1 - X_{BC}) \cdot I_{BC}(V_{BCi}) \\
&I_{BC1x} = X_{BC} \cdot I_T(V_{BC}) / \beta_R, \\
&I_{BC2x} = X_{BC} \cdot I_{BC}(V_{BC}) \\
&I_{BE1} = I_{FT} / \beta_F, \quad I_{BE2} = I_{BE}(V_{BE})
\end{aligned}
\tag{2}
$$

TABLE I
MODEL PARAMETERS USED IN CURRENT SOURCES

I_T	I_{0T}	V_{AT}	n_{0T}	δ_{NT}
I_{BE}	I_{0BE}	V_{ABE}	n_{0BE}	δ_{NBE}
I_{BC}	I_{0BC}	V_{ABC}	n_{0BC}	δ_{NBC}

The junction temperature is calculated according to $T_J = \Theta \cdot P$, where Θ is thermal resistance and P is total dissipated power. Forward and reverse Gummel characteristics measured from 10 to 150°C were used to extract the above-listed dc model parameters. At each temperature, the saturation currents and ideality factors for I_T, I_{BE}, and I_{BC} were extracted together with forward and reverse current gains β_F and β_R. Their temperature dependence was then examined to determine the parameters listed in Table I. The pre-exponential factors (I_{0T}, I_{0BE}, I_{0BC}) and activation energies (V_{AT}, V_{ABE}, V_{ABC}) were extracted from Arrhenius plots of saturation currents. Ideality factors were fitted with straight lines to obtain the n_0 and δ_N parameters. All the extracted dc model parameters were found to be physically reasonable and in agreement with values calculated by using a two-dimensional physical device simulator [2]. β_F and β_R were found to be independent of temperature. Table II summarizes the extraction procedure described above.

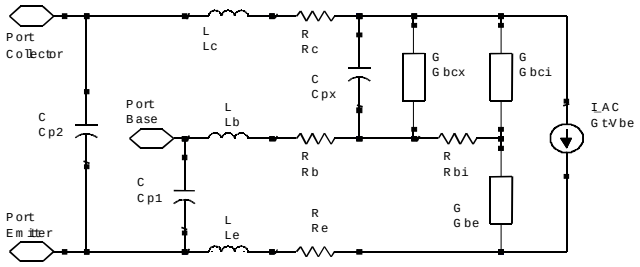

Fig. 3 Small-signal equivalent circuit model.

Thermal resistance Θ and its linear temperature dependence δ_Θ were determined according to the procedure of [1].

TABLE II
DC MODEL PARAMETER EXTRACTION PROCEDURE

Parameters	Extracted from ...	By Using ...
I_{0T}, V_{AT}, n_{0T}, δ_{NT}	forward Gummel	collector current
I_{0BE}, V_{ABE}, n_{0BE}, δ_{NBE}, β_F	forward Gummel	base current
I_{0BC}, V_{ABC}, n_{0BC}, δ_{NBC}, β_R	reverse Gummel	base current

Table III lists typical dc parameter values. Fig. 2 shows that the simulated and measured collector characteristics are in agreement up to a current density of ~2×10^5 A/cm^2.

TABLE III
TYPICAL VALUES OF DC MODEL PARAMETERS

Parameter	Value	Parameter	Value
I_{0T}	1.33 A	I_{0BC}	0.85 A
V_{AT}	1.41 eV	V_{ABC}	0.779 eV
n_{0T}	1.18	n_{0BC}	2.105
δ_{NT}	$-4.30\cdot10^{-4}$ /K	δ_{NBC}	$-4.05\cdot10^{-4}$ /K
I_{0BE}	55 A	β_F	180
V_{ABE}	1.42 eV	β_R	0.35
n_{0BE}	1.23	Θ_0	900 K/mW
δ_{NBE}	$-3.03\cdot10^{-4}$ /K	δ_Θ	1.53 K/mW^2

III. SMALL-SIGNAL MODEL

Fig. 3 shows the small-signal equivalent circuit model. *S*-parameters were measured at different biases and were used to determine the values of small-signal model elements. Extrinsic elements (R_B, R_E, R_C, L_B, L_E, L_C, C_{P1}, C_{P2}, C_{PX}) were assumed independent of bias and were extracted first by using cold-HBT and open-collector methods. Table IV lists the extracted extrinsic element values. These values were then used to de-embed the intrinsic *Y*-parameters in the active region.

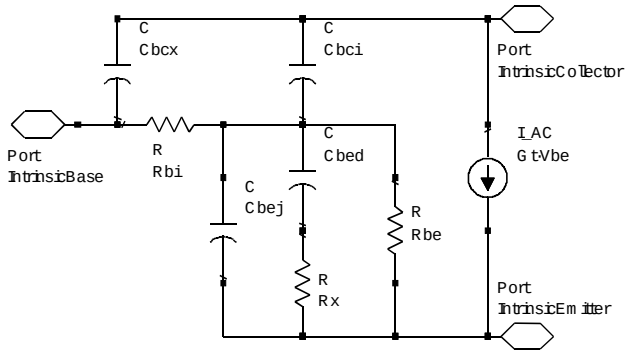

Fig. 4 Circuit representation of intrinsic HBT

TABLE IV
TYPICAL VALUES OF EXTRINSIC ELEMENTS

C_{P1}	75 fF	R_C	1.60 Ω	L_B	76 pH
C_{P2}	60 fF	R_B	1.62 Ω	L_E	57 pH
C_{PX}	18 fF	R_E	1.35 Ω	L_C	27 pH

We have been using a fixed geometric relationship to calculate the five intrinsic elements (R_{Bi}, G_T, G_{BE}, G_{BCx}, and G_{BCi}) from the four *Y*-parameters [3].

$$X_{BC} = \frac{G_{BCx}}{G_{BCi} + G_{BCx}}, \quad G_{BC} = G_{BCi} + G_{BCx},$$

$$G_T = A, \quad G_{BE} = A \cdot \frac{Y_{11} + Y_{12}}{Y_{21} - Y_{12}}, \quad G_{BC} = B,$$

$$R_{Bi} = \frac{1}{B(1 - XBC)} \frac{Y_{12} + Y_{22}}{Y_{11} + Y_{21}}, \tag{3}$$

$$A = \frac{(1 - XBC)(Y_{12} - Y_{21}) \cdot (Y_{11}Y_{22} - Y_{12}Y_{21})}{Y_{11}(Y_{12} + XBC\,Y_{22}) + Y_{12}[Y_{21} + XBC(Y_{12} - Y_{21} + Y_{22})]},$$

$$B = \frac{Y_{11}Y_{22} - Y_{12}Y_{21}}{Y_{11} + Y_{21} + XBC(Y_{12} + Y_{22})}.$$

This approach, although works well under low currents, is not valid under high currents. Under high currents, effects such as base push out and emitter crowding become significant [4] and the ratio of intrinsic and extrinsic base-collector admittances is no longer constant. Therefore, we now propose to fix R_{Bi} to the value extracted under low currents and use such a fixed R_{Bi} to calculate the remaining intrinsic elements under high currents:

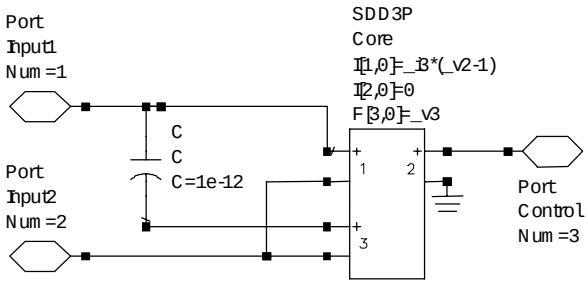

Fig. 5 Implementation of multi-variable capacitor.

$$G_T = C \cdot (Y_{21} - Y_{12}), \quad G_{BE} = C \cdot (Y_{11} + Y_{12}),$$

$$G_{BCx} = \frac{R_{Bi}(Y_{11}Y_{22} - Y_{12}Y_{21}) - Y_{12} - Y_{22}}{R_{Bi}(Y_{11} + Y_{12} + Y_{21} + Y_{22})},$$

$$G_{BCi} = \frac{1}{R_{Bi}} \frac{Y_{12} + Y_{22}}{Y_{11} + Y_{21}}, \tag{4}$$

$$C = \frac{Y_{11} + Y_{12} + Y_{21} + Y_{22}}{[1 - R_{Bi}(Y_{11} + Y_{12})](Y_{11} + Y_{21})}$$

Base-emitter admittance G_{BE} is usually modeled by a simple parallel *R*-*C* circuit. However, under high currents the real part of G_{BE} was found to have non-zero frequency dependence. Therefore, it was necessary to add a resistor R_x in series with the base diffusion capacitor (Fig. 4). G_{BE} was then fitted to:

$$G_{BE} = j\omega C_{BEJ} + \frac{j\omega C_{BED}}{1 + j\omega C_{BED} R_X} + \frac{G_m}{\beta_F} + G_{BE2} \tag{5}$$

where C_{BEJ} is the base-emitter junction capacitance, C_{BED} is the base-emitter diffusion capacitance, and $G_{BE2} = \partial I_{BE2} / \partial V_{BE}$. Using (5) the values of C_{BED} and R_X were extracted at each bias.

IV. LARGE-SIGNAL MODEL

The small-signal model includes multi-variable capacitors (C_{BCi}, C_{BCx}, C_{BED}) that are not merely functions of the voltages across the capacitors. For example, under high currents, C_{BCi} is a function of both V_{BCi} and I_C. Since it is impossible to implement such an element using only bias-dependent charge sources, we now propose a circuit implementation based on the differential equation:

$$I = C_{BCi}(V_{BCi}, I_C) \frac{\partial V_{BCi}}{\partial t} \tag{6}$$

Fig. 5 shows one possible implementation of such an element in a commercially available circuit simulator by using its built-in symbolically defined device [5]. Other multi-variable capacitors can be similarly realized. Such an implementation ensures a logical and bi-lateral

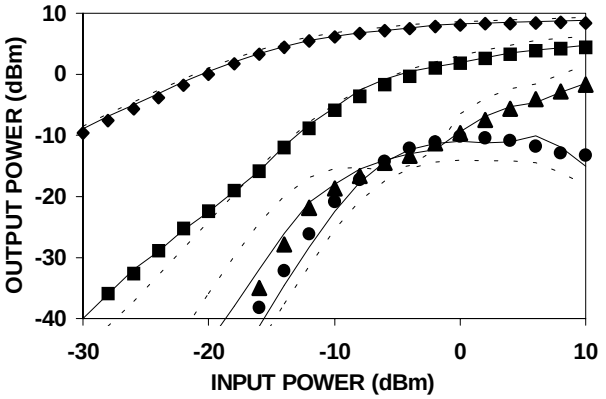

Fig. 6 Simulated by (---) as-extracted and (—) re-optimized model vs. (symbols) measured harmonics of output power. (◆) fundamental frequency at 2 GHz (■) 2nd, (▲) 3rd, and (●) 4th

correlation between small- and large-signal models and avoids the common deficiency of not being able to use the large-signal model to accurately predict small-signal characteristics.

The transconductance G_T can be similarly translated from frequency domain into a differential equation and implemented as another symbolically defined device.

$$G_T = G_m \frac{e^{-j\omega\tau_\varphi}}{1+j\omega\tau_T} \approx G_m \frac{1}{1+j\omega\tau_T} \frac{1-j\omega\frac{\tau_\varphi}{2}}{1+j\omega\frac{\tau_\varphi}{2}} \quad (7)$$

where τ_φ and τ_T are bias-dependent time constants and $G_m = \partial I_{FT}/\partial V_{BEi}$. Thus,

$$I'_{FT} = I_{FT} - \frac{\tau_\varphi}{2}\frac{\partial I_{FT}}{\partial t} - \left(\tau_T + \frac{\tau_\varphi}{2}\right)\frac{\partial I'_{FT}}{\partial t} - \frac{\tau_T\tau_\varphi}{2}\frac{\partial^2 I'_{FT}}{(\partial t)^2} \quad (8)$$

where I_{FT} is defined in (2). I'_{FT} is the actual forward transport current calculated by the model, while taking into account the transfer function (7).

The resulted large-signal model, although too complicated to be fully illustrated here, converges readily even under high-current conditions. By not restricting the model to simple capacitors and current sources, the model preserves device physics through differential equations. This is probably the main reason the as-extracted (without numerical optimization) large-signal model closely predict the performance of HBTs and readily serve as the initial values for further optimization by standard numerical techniques. Fig. 6 illustrates the agreement between measured harmonic output and that simulated by using either the as-extracted model or the re-optimized model.

IV Conclusion

As the supply voltage continues to drop, high-current effects become increasingly important and large-signal HBT models must be valid under high currents. In the present paper, we continue the physics-based analysis of high-current effects of [1] but implement the physical insight in a differential-equation-based large-signal model. Additional innovations were also made in both the small-signal model and the model extraction procedure. The model improvement includes bi-lateral correlation with small-signal characteristics and series resistance with the base-emitter diffusion capacitance. The improvement in extraction procedure is mainly based on a fixed intrinsic vs. extrinsic base-collector capacitance ratio at low currents whereas a fixed intrinsic base resistance at high currents. The model has been implemented in a commercially available circuit simulator by using the so-called symbolically defined devices to represent the physics-based differential equations. Experimentally it has been verified that the as-extracted (without numerical optimization) model closely simulate the RF power performance of the HBTs and can serve as valid initial values for further optimization by using standard numerical techniques. The above-described improvements represent a significant step toward the eventual goal of standard model and automatic extraction for HBTs.

References

[1] M. S. Shirokov, S. V. Cherepko, X. Du, J. C. M. Hwang and D. A. Teeter, "Large-signal modeling and characterization of high-current effects in InGaP/GaAs HBTs," accepted for publication in *IEEE Trans. Microwave Theory Techniques.*

[2] *Atlas,* Silvaco International, Santa Clara, CA 95054 USA.

[3] C. J. Wei and J. C. M. Hwang, "Direct extraction of equivalent circuit parameters for heterojunction bipolar transistors," *IEEE Trans. Microwave Theory Techniques,* vol. 43, pp. 2035-2040, Sep. 1995.

[4] W. Liu, Handbook of III-V Heterojunction Bipolar Transistors, New York: Wiley, 1998, pp. 233-328.

[5] *Advanced Design System,* Agilent Technologies, Westlake Village, CA 91362 USA.